Molecular Dynamics Simulation Study of Water Surfaces: Comparison of Flexible Water Models

Pak K. Yuet*,† and Daniel Blankschtein‡

Department of Process Engineering and Applied Science, Dalhousie University, P.O. Box 1000, Halifax, Nova Scotia, Canada B3J 2X4, and Department of Chemical Engineering, Massachusetts Institute of Technology, Cambridge, Massachusetts 02139, United States

Received: July 19, 2010; Revised Manuscript Received: September 20, 2010

Molecular dynamics (MD) simulation has been used extensively to study water surfaces. Nevertheless, the quantitative prediction of water surface tension has been controversial, since results from different simulation studies using the same water model may differ considerably. Recent research has suggested that bond flexibility, long-range electrostatic interactions, and certain simulation parameters, such as Lennard-Jones (LJ) cutoff distance and simulation time, may play an important role in determining the simulated surface tension. To gain better insight on the MD simulation of water surfaces, particularly on the prediction of surface tension, we examined seven flexible water models using a consistent set of simulation parameters. The surface tensions of the flexible, extended simple point charge (SPCE-F) model and the flexible three-center (F3C) model at 300 K were found to be 70.2 and 65.3 mN/m, respectively, in reasonable agreement with the experimental value of 71.7 mN/m. More importantly, however, detailed analysis of the interfacial structure and contributions from various interactions have revealed that the surface tension of water is determined by the delicate balance between intramolecular (bond stretching) and intermolecular (LJ) interactions, which reflects both the molecular orientation in the interfacial region and the density variation across the Gibbs dividing surface (GDS). In addition, the water molecules on the liquid side of the GDS were found to lie almost parallel to the surface, which helps to clarify the dual-layer structure suggested by sum-frequency generation spectroscopy. By correlating the simulated surface tensions of the seven water models with selected molecular parameters, it was found that the partial charge distribution in the water molecule is likely a key factor in determining the near-parallel alignment of water molecules with the surface.

1. Introduction

The operation of many industrial processes, such as liquid−liquid extraction and gas absorption, relies on the behavior of liquid−liquid or gas−liquid interfaces, and the properties of surfactant-laden interfaces are critical in the formulation of cleansing agents. Surfactants with complex molecular architectures, such as monoalkyl disulfonates and perfluoropolyethers, are used extensively in industrial applications.[1−3] Many of these so-called high-performance surfactants possess unusual interfacial characteristics compared to linear alkyl surfactants such as linear alkyl sulfonates and alkyl ethoxylates. To facilitate the design of interfacial processes such as absorption, and to enhance the use of complex surfactants in industrial applications, it is important to have a detailed understanding of interfaces. Among the many different types of interfaces, the air−water interface, or water surface, is of particular importance because of its prevalence in many industrial systems. The structure of water surfaces has been studied experimentally in the past few decades.[4] Since the early work of Goh et al.,[5] in which the technique of second-harmonic generation was used to probe the orientation of water molecules at the vapor−liquid interface, a considerable amount of research, mostly employing the technique of sum-frequency generation (SFG), has been done on water surfaces.[6−10]

Many of these experimental studies have been summarized by Shen and Ostroverkhov,[11] and the general conclusion is that the water surface is partially ordered and probably contains a distorted hydrogen-bonded network, with some water molecules oriented with a O−H bond pointing into the vapor phase (the so-called "dangling" OH bond). Although SFG spectroscopy has been used extensively to probe interfacial structures, it must be emphasized that the interpretation of the vibrational spectra for water surfaces, particularly the broad band between 3000 and 3600 cm^{-1}, is still a subject of discussion.[7,12−16]

Molecular dynamics (MD) simulation is a powerful technique for studying interfaces at the molecular level. In fact, MD simulation was used in conjunction with many of the experimental studies cited above to enhance the interpretation of the vibrational spectra (see also refs 17−19). In applying this simulation technique, however, it is important that the model system can adequately capture the characteristics of the interface. In the MD simulation of water surfaces, the consistent prediction of surface tension is particularly problematic. A survey of the literature has revealed that simulated surface tensions not only vary with the water models used, but may also depend on parameters such as the Lennard-Jones (LJ) cutoff distance, the treatment of electrostatic interactions, and the simulation time.[20−25] For example, using SPCE water, Ismail et al.[23] obtained a surface tension of 55.4 mN/m at 300 K, while Chen and Smith[25] obtained a value of 61.3 mN/m, and yet other values of approximately 70 mN/m were obtained by Shi et al.[26] and by Lu and Wei.[27] In fact, these differences in simulation

* Corresponding author. Phone: 902-494-3213. Fax: 902-420-7639. E-mail: pak.yuet@dal.ca.
† Dalhousie University.
‡ Massachusetts Institute of Technology.

10.1021/jp1067022
Published on Web 10/12/2010

TABLE 1: Molecular Parameters for the Seven Flexible Water Models Considered in the Present Study

parameter[a]	SPCE-F	SPC-F	SPC-G	SPC-Fw	SPC-Fd	Ferguson	F3C
q_O (e)	−0.8476	−0.78	−0.806	−0.82	−0.82	−0.826	−0.82
σ_O (nm)	0.3166	0.3145	0.3132	0.3166	0.3166	0.3183	0.3166
ϵ_O (kJ/mol)	0.6502	0.6757	0.6926	0.6503	0.6504	0.6926	0.7732
σ_H (nm)	0	0	0	0	0	0	0.082
ϵ_H (kJ/mol)	0	0	0	0	0	0	0.0418
k_b (kJ/mol nm^2)	463826	463700	463700	443153	441077	229074	209200
b_0 (nm)	0.1	0.1	0.0985	0.1012	0.1	0.1	0.1
k_θ (kJ/mol rad^2)	383.0	383.0	383.0	317.57	317.57	417.6	502.08
θ_0 (deg)	109.4	109.47	114.0	113.24	109.5	109.5	109.47
k_{cub} (nm^{-1})	0	0	0	0	0	−16.5	0
k_{UB} (kJ/mol nm^2)	0	0	0	0	33388	0	0
r^0_{HH} (nm)	0	0	0	0	0.1633	0	0
ref	32	28	28	38	39	40	41

[a] q_O: charge on oxygen atom. σ_i, ϵ_i: Lennard-Jones parameters of atom i. k_b: bond-stretching constant. b_0: equilibrium bond length. k_θ: angle-bending constant. θ_0: equilibrium H−O−H angle. k_{cub}: cubic bond-stretching constant. k_{UB}: Urey−Bradley constant. r^0_{HH}: equilibrium distance between the two H atoms in a water molecule.

parameters used in previous simulations of water surfaces make any direct comparison of water models rather difficult.

One of the molecular parameters which may affect the simulated water surface tension is the flexibility of the O−H bond. The inclusion of bond flexibility in the simulation of bulk water has long been a subject of debate. For example, in a study based on the simple point charge (SPC) model, Tironi et al. concluded that the addition of bond flexibility in the simulation of bulk water is not warranted,[28] but an earlier study by Teleman et al. using a similar model seemed to suggest otherwise.[29] A comprehensive discussion on bond flexibility, including its effect on the molecular dipole moment, can be found in an excellent review by Wallqvist and Mountain.[30] The role of bond flexibility in the simulation of water surfaces has been investigated only recently. For example, Raabe and Sadus found that bond flexibility may affect the simulated vapor−liquid equilibrium,[31] and López-Lemus et al. also observed a considerable effect of bond flexibility on simulated water surface tension.[32] Earlier flexible water models are based on the central force concept, which does not distinguish between intermolecular and intramolecular potentials.[33] More recent models, however, include explicit intermolecular and intramolecular terms, and some of them were developed without reparametrization. For example, Toukan and Rahman[34] used a quadratic intramolecular potential with force constants taken from the model by Kuchitsu and Morino.[35] The study by López-Lemus et al.[32] cited above was based on the SPCE model, augmented with harmonic bond-stretching and bending potentials (hereafter referred to as "SPCE-F"), using parameters taken from the models developed by Tironi et al.[28] Amira et al.[36] also developed a model based on SPC water, using a quartic intramolecular potential developed by Carney et al.[37]

With all of the above in mind, the primary objectives of the present study are (i) to compare various flexible water models using a common set of simulation parameters, with particular emphasis on their ability to predict surface tension, and (ii) to develop a better understanding of water surface tension in relation to the interfacial molecular structure. For these purposes, seven flexible water models were considered in this study, where all but SPCE-F were developed with reparameterization of the SPC configuration. More specifically, the "SPC-F" and "SPC-G" models by Tironi et al.,[28] as well as the "SPC-Fw" model by Wu et al.,[38] incorporate harmonic bond-stretching and angle potentials into SPC water. Dang and Pettitt, on the other hand, used a harmonic bond-stretching potential and the Urey−Bradley (UB) angle potential with SPC (hereafter referred to as "SPC-Fd").[39] In the model developed by Ferguson, a cubic term was included in the bond-stretching potential, and the atomic charges on the oxygen and hydrogen atoms were slightly different from those in SPC water.[40] Levitt et al. developed the "F3C" model for use with the Encad force field, which uses a special shift function to allow for a rapid truncation of the LJ and Coulombic potentials.[41] In addition to their relative simplicity, the selection of these seven models was intended to provide sufficient variation for extracting useful information on the effect of bond flexibility on the simulation of water surfaces. It should be noted that many other rigid and flexible water models do exist, and some of them have been used for the study of water surfaces (see, for example, refs 42 and 43 and references cited therein). However, an exhaustive review of these models is beyond the scope of the present study, and interested readers are referred to other sources, such as refs 30 and 33 and references cited therein, for more details.

The remainder of this paper is organized as follows: section 2 provides the details of the water model, system configuration, and simulation parameters and procedure, as well as the methodology used to analyze the results. The simulation results are presented and discussed in section 3, and finally, concluding remarks are presented in section 4.

2. Method

The molecular parameters of the seven water models selected for this study are summarized in Table 1. As stated earlier, the models are based on the SPC configuration, with the charge distribution characterized by the partial charge, q_O, on the oxygen atom. All models, except F3C, have their LJ interaction sites on the oxygen atom only, as characterized by the LJ parameters, σ_O and ϵ_O. For F3C, LJ interactions also occur through the hydrogen atoms (σ_H and ϵ_H in Table 1). Bond flexibility in all water models, except the Ferguson model, is characterized by a harmonic bond-stretching potential, $V_b(r)$, given by

$$V_b(r) = \frac{1}{2}k_b(r - b_0)^2 \quad (1)$$

where k_b is the bond-stretching constant, r is the O−H bond length, and b_0 is its equilibrium value. An additional cubic term is included in the Ferguson model, that is[40]

$$V_b(r) = k_b(r - b_0)^2 + k_b k_{cub}(r - b_0)^3 \quad (2)$$

where k_{cub} is the cubic bond-stretching constant. The angle-bending potential, $V_\theta(\theta)$, in all models, except SPC-Fd, is also characterized by the harmonic form, that is

$$V_\theta(\theta) = \frac{1}{2}k_\theta(\theta - \theta_0)^2 \quad (3)$$

where k_θ is the angle-bending constant, θ is the H−O−H angle, and θ_0 is its equilibrium value. The Urey−Bradley potential is used in SPC-Fd, namely[39]

$$V_\theta(\theta) = \frac{1}{2}k_\theta(\theta - \theta_0)^2 + \frac{1}{2}k_{UB}(r_{HH} - r^0_{HH})^2 \quad (4)$$

where k_{UB} is a constant, r_{HH} is the distance between the two H atoms, and r^0_{HH} is the corresponding equilibrium value.

Simulation Procedure. All simulations were performed using the GROMACS package (version 4.0).[44,45] A simulation cell of 5 nm × 5 nm × 5 nm was first filled with 4142 water molecules using the spc216.gro file provided with GROMACS. Note that the size of this system is larger than those used in many recent simulation studies of interfacial systems (see, for example, refs 25, 46−48). One notable exception is the study by Fan et al.,[9] who used a system containing 8049 water molecules. A preliminary test run using 8225 rigid SPCE water molecules was also performed in the present study, which yielded a simulated surface tension similar to that obtained with 4142 molecules (data not shown). A 500 ps constant-NP_zT simulation (time step = 1 fs) was performed in which the pressure along the z-axis, P_z, is kept at 1 bar using a τ_P of 0.5 ps, where τ_P is the time constant for the Berendsen pressure coupling. The water molecules were then centered in a 5 nm × 5 nm × 25 nm box, with the two surfaces perpendicular to the z-axis, which allows for a vacuum of approximately 10 nm on each side of the water layer (see Figure 1a). Note that this space will hereafter be referred to as the vapor phase, since some water molecules escaped from the water layer during the simulation. It is worth noting that different box geometries have been used to study interfacial systems, usually with $L_x = L_y = L_z/\alpha$, where L_x, L_y, and L_z are the x, y, and z dimensions, respectively, and α ranges from 3 to 7.[9,46−49] A constant-NVT equilibration was then performed for 1 ns, followed by a 5 ns constant-NVT production run, all with a time step of 1 fs.[25] Velocity rescaling was used in all cases to maintain the system temperature at 300 K, with a time constant, τ_T, equal to 0.2 ps.[50]

As mentioned earlier, simulated water surface tension has been found to depend, albeit weakly, on the LJ cutoff distance, r_c.[23,24,51] Therefore, to allow for a systematic comparison of the seven water models considered, all simulations in the present study were performed using a simple cutoff with $r_c = 2.45$ nm, approximately half of the box width. Such an unusually large r_c value was selected to minimize the possible adverse effect of a small r_c value on the simulated surface tension reported in the literature.[23,24,51] It may be argued that a large and uniform r_c is perhaps inconsistent with some of the water models. For example, the F3C model was originally developed using a short cutoff, coupled with a special shift function, to reduce the computational requirement, and it was found that a r_c value of 0.6−1.0 nm was satisfactory for simulating bulk water.[41,52] However, it must be emphasized that all the water models considered in the present study were developed for bulk water simulation, and the role of r_c in determining the surface tension of flexible water models has not been studied thoroughly. The validity of using a long cutoff in the present study for simulating water surfaces can therefore only be assessed a posteriori. The particle-mesh Ewald (PME)[53] summation technique was used to account for the long-range electrostatic interactions, with a grid spacing of 0.12 nm, a real-space cutoff equal to r_c, and the tinfoil boundary conditions.[54] Periodic boundary condition was applied to all three directions.

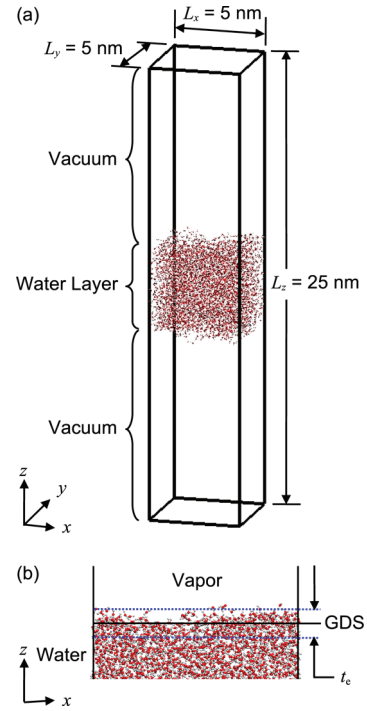

Figure 1. (a) Initial configuration of the simulation cell. (b) Details of the upper surface showing the Gibbs dividing surface (GDS) and the "10−90" interface width, t_e.

Data Analysis. All data analyses were performed using the 5 ns production run. Surface tension, γ, can be defined in terms of the difference between the normal (z-direction) and lateral components of the pressure tensor. For the configuration used in this study in which a simulation cell of length L_z contains two surfaces, γ can be expressed as follows:[55,56]

$$\gamma = \frac{1}{2}\int_0^{L_z}[P_{zz} - 0.5(P_{xx} + P_{yy})]\,dz \quad (5)$$

where P_{xx}, P_{yy}, and P_{zz} are the three diagonal components of the pressure tensor along the x-, y-, and z-direction, respectively. The values of γ reported in section 3 were determined using the g_energy analysis program supplied with GROMACS. The pressure tensor, $\mathbf{P}$, is related to the virial tensor via the following relation[57,58]

$$\mathbf{P} = \frac{1}{V}(2\mathbf{E} + \boldsymbol{\Xi}) \quad (6)$$

where V is the system volume, $\mathbf{E}$ is the kinetic-energy tensor, and $\boldsymbol{\Xi}$ is the atomic virial tensor. Defining $\Delta P = P_{zz} - 0.5(P_{xx} + P_{yy})$, we can write, from eq 6, $\Delta P = (2\Delta E + \Delta\Xi)/V$, where ΔE is defined as $\Delta E = E_{zz} - 0.5(E_{xx} + E_{yy})$. The atomic virial tensor is defined as follows:[59]

$$\Xi = \sum_{i=1}^{n} \mathbf{F}_i \otimes \mathbf{r}_i \tag{7}$$

where $\mathbf{F}_i$ is the force acting on atom i, $\mathbf{r}_i$ is the position of atom i, n is the total number of atoms, and $\otimes$ denotes a direct product. For a flexible water model, $\mathbf{F}_i$ is composed of four components due to (i) the Lennard-Jones interactions (LJ), (ii) electrostatic interactions (qq), (iii) bond stretching (b), and (iv) angle bending (θ). Accordingly, the difference between the normal and lateral components of the virial tensor can be written as follows:

$$\Delta\Xi = \sum_m \Delta\Xi_m = \sum_m [\Xi_{m,zz} - 0.5(\Xi_{m,xx} + \Xi_{m,yy})] \tag{8}$$

where the index m denotes the various components (LJ, qq, b, or θ), and the subscripts xx, yy, and zz denote the three diagonal components of the virial tensor along the x-, y-, and z-direction, respectively. Note that ΔE tends to be much smaller than $\Delta\Xi$, which implies that the surface tension, as expressed in eq 5, is dominated by $\Delta\Xi$. Indeed, the contribution of ΔE to γ is only about 1% (data not shown); consequently, the discussion on surface tension presented in section 3 may be focused on the virial difference without loss of generality.

The quantities $\Delta\Xi_{LJ}$, $\Delta\Xi_b$, and $\Delta\Xi_\theta$ can be calculated based on the interactions between atom pairs. The calculation of the electrostatic component, however, is not as straightforward, since the PME approach to calculating electrostatic interactions does not allow a simple decomposition into pairwise forces.[59] Since the virial differences are used in this study mainly for comparison purposes, the quantity $\Delta\Xi_{qq}$ was approximated using only the direct Coulombic interactions within the central simulation cell.[60] As stated earlier, the simulated surface tension values reported here were calculated using the g_energy analysis program, which utilizes the full electrostatic forces based on the PME approach. However, it is worth noting that the surface tensions estimated using the approximate $\Delta\Xi_{qq}$ and eqs 5 and 6 are similar to those obtained using the g_energy program (data not shown). To determine the variation of $\Delta\Xi_m$ along the z-axis, we adopted the approach proposed by Lindahl and Edholm.[59,61] Briefly, the simulation cell was divided into 250 slabs along the z-direction, each 0.1 nm thick, as suggested in ref 59. A local pressure tensor similar to that given in eq 6 can be defined for each slab, with the contribution from the virial tensor distributed according to the relative location of the interacting particles.

To investigate the details of the water structure, particularly the molecular orientation in the interfacial region, two commonly used quantities were calculated: (i) the water dipole order parameter, $\langle\cos\theta\rangle$, and (ii) the probability distributions, $P(\theta_{OH})$ and $P(\theta_{Oe})$. In the present study, θ is defined as the angle between the water dipole and the positive z-axis (see Figure 2a), while θ_{OH} is defined as the angle between the O−H bond and the normal vector, **n**, pointing into the water layer and perpendicular to the interface (see Figure 2b). Similarly, θ_{Oe} is the corresponding angle formed with the hypothetical "bond" between the oxygen atom and the lone-pair electrons ("O−e bond").[62−64] Therefore, θ_{OH} (θ_{Oe}) is zero when the O−H bond (O−e bond) is pointing perpendicularly into the water layer. The water dipole order parameter in each slab was calculated as $\langle\cos\theta\rangle = \langle(\sum_{i=1}^{n}\cos\theta_i)/n\rangle$, where n is the number of molecules in the slab. The geometry of the O−e bond was taken as that of the ST2 water model developed by Stillinger and Rahman,[65]

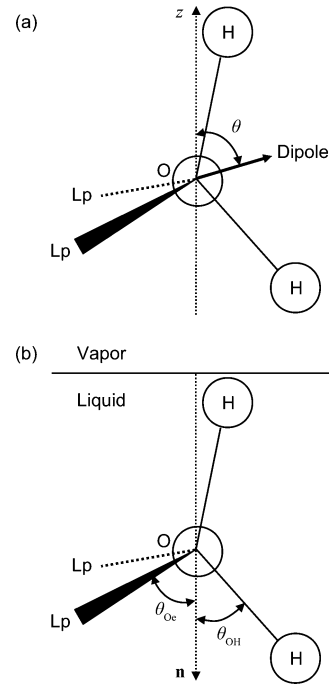

Figure 2. Schematic diagrams showing (a) the angle θ between the water dipole and the positive z axis, and (b) the angles θ_{OH} and θ_{Oe} between the inward normal vector, N, and the O−H and O−e bonds, respectively. "Lp" denotes the lone-pair electrons.

and the probability distributions were calculated for the layers above and below the Gibbs dividing surface (GDS), each having a thickness of $t_e/2$, where t_e is the "10−90" interface width, which is commonly used to characterize the thickness of the interfacial region (see Figure 1b and the discussion below).

In addition to the quantities described above, the density profile and the dielectric constant of the water layer were also calculated in the present study. These two quantities were used, together with the surface tension, to assess the accuracy of the simulations by comparing to experimental data. As discussed below, the density profile was also used to determine the location of the GDS. On the other hand, the dielectric constant is a potentially important property, particularly in studying the behavior of ionic surfactants adsorbed on water surfaces. In such cases, the dielectric constant of the water layer may play a key role in regulating the electrostatic interactions between these surfactants. The density profile, $\rho(z)$, was determined by fitting an error function of the following form[56,66]

$$\rho(z) = \frac{\rho_l + \rho_v}{2} - \frac{\rho_l - \rho_v}{2}\,\mathrm{erf}\left(\frac{z - z_0}{\sqrt{2}d_e}\right) \tag{9}$$

where ρ_l is the liquid density, ρ_v is the vapor density, z_0 is the midpoint of the interface, or the location of the GDS, and d_e is a parameter related to t_e by $t_e = 2.5631d_e$. As noted by Mountain, however, the accuracy of the fitted ρ_v tends to be poor.[46] Consequently, in the present study, ρ_v was estimated by taking the time average of the simulated densities in the vapor phase. Note that similar results were obtained by fitting a hyperbolic tangent function, which is also often used to characterize the density profile across an interface.[46,66]

The dielectric constant, or relative permittivity, of the water layer was calculated using the expression derived by Ballenegger and Hansen.[67] More specifically, for each slab of the simulation

TABLE 2: Simulated Surface Tension (γ), "10−90" Interface Width (t_e), Liquid Density (ρ_l), Vapor Density (ρ_v), Average Dipole Moment (μ), and the Parallel Component of the Permittivity Tensor ($\epsilon_{||}$) for the Seven Flexible Water Models Considered[a]

	$\gamma \pm$ s.d.[b] (mN/m)	t_e (nm)	ρ_l (g/cm^3)	ρ_v (g/cm^3)	μ (D)	$\bar{\epsilon}_{||}$
SPCE-F[c]	70.2 ± 2.1	0.34	1.026	4.003×10^{-7}	2.55	112.1
F3C	65.3 ± 1.5	0.37	1.000	6.249×10^{-6}	2.46	95.0
SPC-Fw	63.4 ± 1.0	0.37	1.008	5.604×10^{-6}	2.39	79.5
SPC-Fd	62.1 ± 1.5	0.38	1.006	8.147×10^{-6}	2.45	106.2
Ferguson	60.6 ± 1.3	0.38	0.993	4.003×10^{-6}	2.46	98.3
SPC-G	54.0 ± 0.9	0.43	0.999	4.979×10^{-5}	2.22	63.9
SPC-F	52.5 ± 1.1	0.44	0.988	5.085×10^{-5}	2.30	84.2
expt	71.7[68]	−	0.9965[69]	2.55×10^{-5} [75]	2.9[76]	78.4[70]

[a] All simulations were performed at 300 K. t_e and ρ_l were determined by fitting the density profile, $\rho(z)$, to an error function (see text for details); ρ_v was estimated by averaging the densities in the vapor phase. [b] The standard deviation (s.d.) was estimated by dividing the 5 ns production run into 10 0.5 ns blocks. [c] A simulation of rigid SPCE water using the same simulation parameters and procedure yielded a surface tension of 60.7 mN/m.

cell, the parallel ($x-y$ plane) component of the permittivity tensor, $\epsilon_{||}$, can be expressed as follows:

$$\epsilon_{||} = 1 + \frac{\langle \mathbf{m}_{||} \cdot \mathbf{M}_{||} \rangle - \langle \mathbf{m}_{||} \rangle \cdot \langle \mathbf{M}_{||} \rangle}{2kTV\epsilon_0} \tag{10}$$

where k is the Boltzmann constant, T is the absolute temperature, ϵ_0 is the permittivity in vacuum, and V is the volume of each slab. The quantity $\mathbf{m} = \sum_{i=1}^{N} \mu_i$ is the total dipole moment in volume V, where $\mu_i = \sum_k q_{i,k} \mathbf{r}_{i,k}$ is the dipole moment of molecule i, N is the total number of water molecules in volume V, $q_{i,k}$ and $\mathbf{r}_{i,k}$ are the charge and position, respectively, of atom k in molecule i, and the summation in μ_i runs over all atoms in the molecule. The total dipole moment in the entire water layer, $\mathbf{M}$, is defined in a corresponding manner. Note that $\langle \mathbf{m}_{||} \cdot \mathbf{M}_{||} \rangle = \langle m_x M_x + m_y M_y \rangle$ and $\langle \mathbf{m}_{||} \rangle \cdot \langle \mathbf{M}_{||} \rangle = \langle m_x \rangle \langle M_x \rangle + \langle m_y \rangle \langle M_y \rangle$. A corresponding expression was derived for the perpendicular (z-direction) component of the permittivity tensor, $\epsilon_\perp$; however, as discussed in ref 67 the dipole moment fluctuation in the z-direction is much smaller than that along the $x-y$ plane, making the determination of $\epsilon_\perp$ very difficult. Indeed, in our simulations, $\epsilon_\perp$ often took on unphysical (negative) values; consequently, only $\epsilon_{||}$ was determined in the present study. Since $\epsilon_\perp$ is, in principle, equal to $\epsilon_{||}$ in an isotropic medium, $\epsilon_{||}$ should provide an accurate measure of the dielectric constant of the bulk water layer. The average dipole moment in the liquid phase, μ, was determined as $\mu = \langle M/N_T \rangle$, where N_T is the total number of water molecules in the water layer.

3. Results and Discussion

The main results of this study are summarized in Table 2. A value of 70.2 mN/m was obtained for the surface tension of the SPCE-F model, which is consistent with that obtained by López-Lemus et al.[32] Among the seven flexible water models, this value provides the best agreement with the experimental value, γ_0, of 71.7 mN/m;[68] however, the surface tension of F3C (65.3 mN/m) is only about 9% lower than γ_0. In contrast, the surface tensions of the SPC-F and SPC-G models are 25−27% below γ_0. Also shown in Table 2 are the average dielectric constants, $\bar{\epsilon}_{||}$, for the seven water models, which were calculated by averaging the $\epsilon_{||}$'s of all the slabs bounded by the two GDSs.

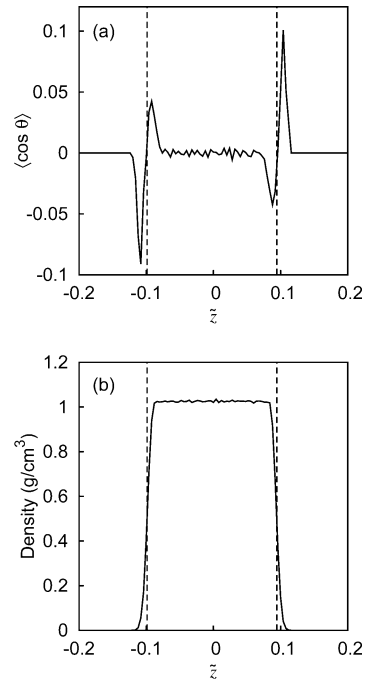

Figure 3. Profiles of (a) water dipole order parameter, $\langle \cos \theta \rangle$, and (b) density for the SPCE-F water model. The Gibbs dividing surfaces are denoted by the two vertical dashed lines.

As a comparison, Wu et al. obtained the dielectric constants of 102.0, 79.6, and 101.8 for the F3C, SPC-Fw, and SPC-Fd models, respectively, using 216 molecules with a r_c of 0.9 nm.[38] Although SPCE-F provides the best agreement with experiment in terms of surface tension, its liquid density of 1.026 g/cm^3 is about 3% higher than the experimental value of 0.9965 g/cm^3 at 27 °C,[69] and its dielectric constant (112.1) is also much higher than the experimental value of 78.4 for bulk water.[70] This observation suggests that careful consideration is required in selecting a proper water model for simulating interfacial systems, particularly in cases involving electrolytes or ionic surfactants. In addition to the properties shown in Table 2, the variations of dipole moments and hydrogen bond populations across the water surface are also provided for the interested readers as Supporting Information.

Water Surface Characteristics. Before comparing the water models in more detail, it may be instructive to examine the general characteristics of the simulated water surface. The SPCE-F model is selected for this purpose because of its excellent agreement with the experimental surface tension. Figure 3a depicts the variation of the water dipole order parameter, $\langle \cos \theta \rangle$, as a function of $\tilde{z}$, where $\tilde{z} = z/L_z - 0.5$. The locations of the GDSs, as obtained by fitting the density profile shown in Figure 3b to eq 9, are denoted by the two vertical dotted lines. The average value of zero for $\langle \cos \theta \rangle$ within the water layer indicates that the water dipoles are randomly distributed, whereas a positive and negative value indicates that the water dipoles are, on average, pointing toward the positive and negative z-direction, respectively (see Figure 1). As shown in Figure 3a, on the vapor side of the GDS, i.e., $\tilde{z}$ just below −0.1 and above 0.1, the water dipoles point toward the vapor phase (see Figure 1). In contrast, on the liquid side of the GDS, the water dipoles point slightly toward the liquid phase. Note that $\langle \cos \theta \rangle \approx 0.04$ corresponds to $\theta \approx 88°$, suggesting that the liquid-side water dipoles are, in fact, almost parallel to the surface.

The simulated probability distributions, $P(\theta_{OH})$ and $P(\theta_{Oe})$, are depicted in Figure 4. As shown in Figure 4a, a broad peak

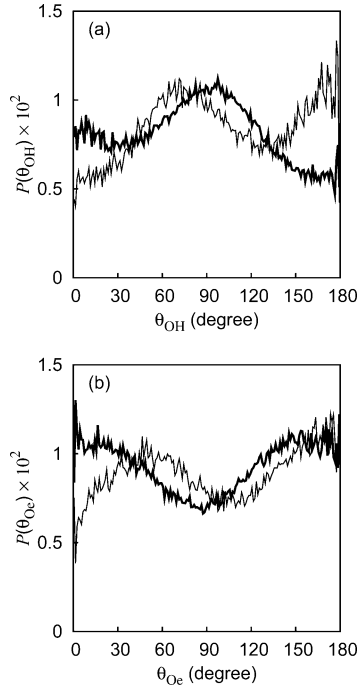

Figure 4. Simulated probability distributions of (a) θ_{OH} and (b) θ_{Oe} on the liquid side (thick line) and the vapor side (thin line) of the Gibbs dividing surface corresponding to the SPCE-F water model. A value of zero for θ_{OH} or θ_{Oe} indicates that the bond is pointing into the liquid phase (perpendicular to the surface).

in $P(\theta_{OH})$ is observed at approximately 90° on the liquid side of the GDS (thick line), whereas the probability distribution of θ_{Oe} (thick line in Figure 4b) suggests that θ_{Oe} generally prefers the values of approximately 15°−30° and 140°−160° on the liquid side. This indicates that the water molecules on the liquid side of the GDS tend to lie parallel to the surface, which is consistent with the result shown in Figure 3. The molecular orientation on the vapor side of the GDS is quite different from that on the liquid side. As depicted by the thin line in Figure 4a, two peaks are observed in $P(\theta_{OH})$ at approximately 70° and 170°, and in $P(\theta_{Oe})$ (thin line in Figure 4b) at slightly lower values (at approximately 50° and between 160° and 180°), which suggests that the water molecules orient themselves with either an O−H bond or an O−e bond pointing toward the vapor phase, tilting slightly from the z-axis. However, because $P(\theta_{OH})$ tends to be smaller in the lower angular range (between 0 and 50°), it is more likely to find an O−H bond pointing toward the vapor phase (away from the interface).

This picture of dual water layers around the GDS, with molecules adopting different orientations, was also observed in a recent study by Fan et al., using both the SFG technique and MD simulations with rigid SPCE water.[9] However, as noted earlier, while there is general agreement that the water molecules on the vapor side of the GDS orient themselves with a dangling O−H bond pointing into the vapor phase, the precise structure on the liquid side of the GDS is still not well established experimentally, mainly because of the uncertainty involved in interpreting the vibrational spectra. Our simulation based on the SPCE-F water model suggests that the water molecules on the liquid side of the GDS tend to lie almost parallel to the surface, which is in good agreement with the conceptual picture suggested by Matsumoto and Kataoka.[71] Interestingly, in contrast to SPC-based water models, the water model used in the study by Matsumoto and Kataoka was based on the MCY potential developed by Matsuoka et al.[72] using ab initio calculations, with the parameters refitted by Carravetta and Clementi.[73]

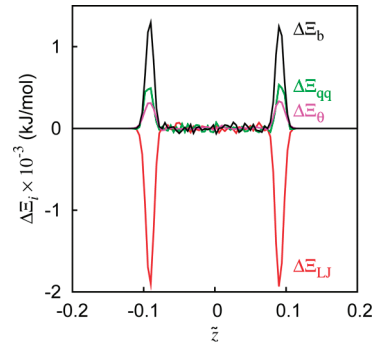

Figure 5. Simulated virial differences, $\Delta\Xi_i$, due to various interactions for the SPCE-F water model. The subscript i denotes LJ interactions ("LJ", red), electrostatic interactions ("qq", green), bond stretching ("b", black) and angle bending ("θ", magenta).

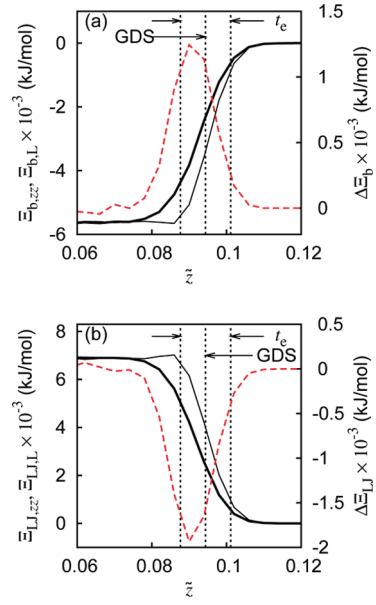

Figure 6. Simulated normal (thick solid line, subscript "zz") and lateral (thin solid line, subscript "L") components of (a) bond-stretching, and (b) LJ virials across a water (SPCE-F) surface. The lateral component is defined as $\Xi_{m,L} = 0.5(\Xi_{m,xx} + \Xi_{m,yy})$, where m denotes the bond-stretching (subscript "b") or LJ (subscript "LJ") contribution. The virial difference (red dashed line) is defined as $\Delta\Xi_m = \Xi_{m,zz} - \Xi_{m,L}$.

To discern the contributions of various bonded and nonbonded interactions to the surface tension, the four components of $\Delta\Xi$ are plotted in Figure 5 for the SPCE-F model. It is clear from the figure that the total virial difference depends on the delicate balance between the contribution from the LJ interactions, and those from the bond-stretching, angle-bending, and electrostatic interactions. In particular, the large negative value of $\Delta\Xi_{LJ}$ (red line) tends to counteract the large positive value of $\Delta\Xi_b$ (black line). Because of its relatively minor contribution to the total virial difference, $\Delta\Xi_\theta$ will not be considered any further. The contribution from electrostatic interactions, however, will be revisited later in discussing the roles of molecular parameters. As shown in Figure 6a, both the normal ($\Xi_{b,zz}$) and lateral ($\Xi_{b,L} = 0.5(\Xi_{b,xx} + \Xi_{b,yy})$) components of the bond-stretching virial are negative. Since the force exerted on a particle is equal to the negative of the potential gradient, a negative bond-stretching virial indicates that the O−H bonds are being stretched (see eq 1). More importantly, within the interfacial region, i.e., the width t_e, the lateral component is more negative than the normal component, resulting in the virial difference reaching a maximum (red dashed line, Figure 6a) on the liquid side of the GDS.

This can be attributed to the fact that, as discussed above, the water molecules on the liquid side of the GDS tend to lie parallel to the water surface, making the magnitude of the lateral component of the bond-stretching virial ($\Xi_{b,L}$) larger than that of the normal component ($\Xi_{b,zz}$).

In the case of the LJ virial, the difference between the normal and the lateral components results in a minimum $\Delta\Xi_{LJ}$ located on the liquid side of the GDS (red dashed line, Figure 6b). This difference reflects the density asymmetry across the GDS, as depicted by the density profile shown in Figure 3; in other words, there are simply fewer water molecules on the vapor side of the GDS. Interestingly, both virial components are positive, indicating that the LJ interactions are, in fact, dominated by repulsive forces.[74] This observation appears to be counterintuitive at first glance; indeed, a simple analysis reveals that the ratio $\langle n_r\rangle/\langle n_a\rangle$, where $\langle n_r\rangle$ and $\langle n_a\rangle$ are the average numbers of repulsive and attractive pairs, respectively, is only about 0.003. Our result therefore indicates that, in spite of the relatively small number of O−O pairs that are experiencing a repulsive LJ force, its total magnitude is still larger than that of the attractive LJ force. This observation seems to suggest that interactions other than the LJ interactions may play a more important role in determining the molecular arrangement in the interfacial region. Indeed, as discussed in a later section, electrostatic interactions caused by the partial charge distribution in the water molecule may be a key factor affecting the orientation of the surface water molecules.

The behavior of the LJ and bond-stretching virials also illustrates the complex nature of the water surface. Conceptually, when the normal component of the pressure tensor is larger than the lateral component, the interfacial layer tends to expand in the normal direction, resulting in the development of a lateral tension in $x-y$ plane. As shown in Figure 6b, within the interfacial region, the LJ interactions enhance the lateral pressure component, compared to the normal component, mainly because of the lower density on the vapor side of the GDS. In contrast, with the water molecules lying almost parallel to the surface, the stretching of the O−H bond acts to reduce the lateral pressure component, resulting in a positive contribution to the surface tension (positive $\Delta\Xi_b$, see Figure 6a). Consequently, the surface tension of water reflects two levels of molecular ordering: (i) the preferred molecular orientation in the interfacial region, and (ii) the density variation across the interface. Both intramolecular (bond stretching) and intermolecular (LJ) interactions contribute to the surface tension, although their effects tend to oppose each other.

Comparison of Water Models. As noted earlier, previous studies have suggested that bond flexibility may be an important factor in determining the simulated surface tension of a water model.[32] Indeed, the preceding analysis of SPCE-F water has clearly identified the contribution of bond stretching to surface tension. However, bond flexibility alone does not seem to be able to account for the range of simulated surface tensions shown in Table 2. In particular, the SPCE-F, SPC-F, and SPC-G models have similar bond-stretching constants, k_b (see Table 1), yet their surface tensions differ by approximately 17 mN/m. Figure 7 depicts the virial differences due to bond stretching, $\Delta\Xi_b$, as a function of $\tilde{z}$ for the three water models. Note that on the liquid side of the GDS ($\tilde{z} \approx \pm 0.1$), $\Delta\Xi_b$ for the SPCE-F model is about 2.3 times that for the SPC-F or SPC-G model, in spite of the similarity in their k_b values as noted above. This difference in $\Delta\Xi_b$ appears to be related to both the stretching and the orientation of the O−H bond. As shown in Figure 8a, the average O−H bond stretching, $\langle r_{OH}/b_0 - 1\rangle$, where r_{OH} is the length of

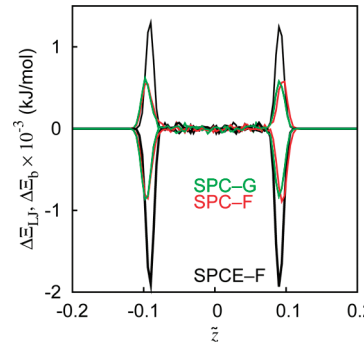

Figure 7. Simulated virial differences due to LJ interactions ($\Delta\Xi_{LJ}$) and bond stretching ($\Delta\Xi_b$) as a function of position, $\tilde{z}$, across the water layer. Black line, SPCE-F; red line, SPC-F; green line, SPC-G. All $\Delta\Xi_{LJ}$ are negative and all $\Delta\Xi_b$ are positive.

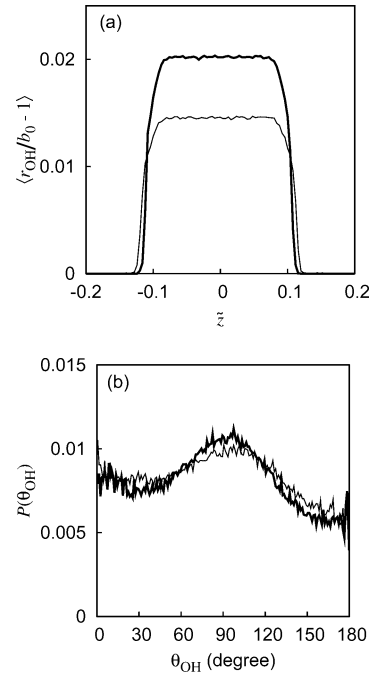

Figure 8. (a) Simulated average bond stretching, $\langle r_{OH}/b_0 - 1\rangle$, as a function of position, $\tilde{z}$, across the water layer. (b) Simulated probability distribution, $P(\theta_{OH})$, on the liquid side of the Gibbs dividing surface. Thick line, SPCE-F water model; thin line, SPC-F water model.

the O−H bond, is larger in the SPCE-F water model (thick line) than in the SPC-F water model (thin line). In addition, as shown in Figure 8b, which depicts the probability distribution of θ_{OH} on the liquid side of the GDS, the peak at approximately 90° for the SPCE-F model (thick line) is slightly higher than that for the SPC-F water model (thin line), suggesting that the water molecules in the SPCE-F model are more aligned with the interface.

The difference in the interfacial liquid water structure between SPCE-F and SPC-F can be further assessed using the radial distribution function, $g_{OO}(r)$, where r is the separation distance between two oxygen atoms. Figure 9 depicts the $g_{OO}(r)$ in the liquid layer adjacent to the GDS, with the thickness of the layer taken as half of the "10−90" thickness shown in Table 2. As depicted in Figure 9, both distribution functions show the first peak at $r = 0.26$ nm, but the value of $g_{OO}(r)$ for SPCE-F (thick line) is higher than that for SPC-F (thin line). The second and third peaks for SPCE-F are also higher than the corresponding peaks for SPC-F, and they are located at shorter distances. This behavior suggests that the interfacial water layer in the SPCE-F

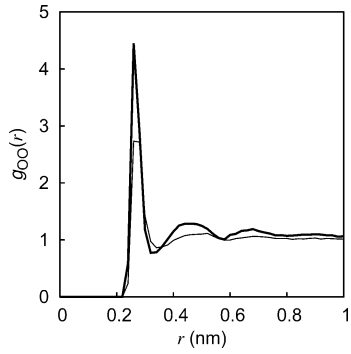

Figure 9. Simulated oxygen−oxygen radial distribution function, $g_{OO}(r)$, in the interfacial liquid layer adjacent to the GDS. Thick line, SPCE-F water model; thin line, SPC-F water model.

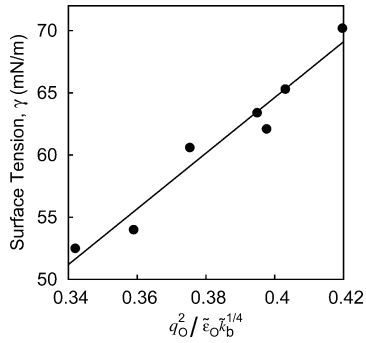

Figure 10. Variation of simulated water surface tension as a function of the ratio $q_O^2/\tilde{\epsilon}_O\tilde{k}_b^{1/4}$, where $\tilde{\epsilon}_O = \epsilon_O/RT$ and $\tilde{k}_b = k_b b_0^2/RT$. The solid line is a linear fit to the data.

model forms a tighter and more rigid structure, compared to that in the SPC-F model. This picture of a tighter, more rigid, "skin" of water layer is consistent with the much sharper interface found in the SPCE-F model (smaller t_e; see Table 2), which is also reflected by the more negative value of $\Delta\Xi_{LJ}$ for SPCE-F shown in Figure 7.

Roles of Molecular Parameters. The analysis of the SPCE-F, SPC-F, and SPC-G water models presented above has highlighted the contributions of LJ and bond-stretching interactions to the water surface tension, which is consistent with the findings of Lopéz-Lemus and co-workers.[32] However, such an analysis has also revealed that models with similar bond-stretching constant, k_b, can produce very different surface tensions. It is worth noting that both surface tension and the virial tensor reflect the interfacial water structure, which is ultimately determined, at least in principle, by the molecular parameters of the water models. Consequently, in comparing the models listed in Table 1, a key question is how the molecular parameters affect the simulated surface tension.

As shown in Table 1, the charge distributions of the SPC-Fw, SPC-Fd, Ferguson, and F3C water models, as characterized by q_O, are very similar, yet their surface tensions vary from 60.6 to 65.3 mN/m (see Table 2), a range that falls between SPCE-F ($q_O = -0.8476e$) and SPC-F ($q_O = -0.78$ e) or SPC-G ($q_O = -0.806e$). This observation suggests that water surface tension may be affected by a combination of molecular parameters. Indeed, Figure 10 depicts a near linear relation between the simulated surface tension, γ, and the ratio $q_O^2/\tilde{\epsilon}_O\tilde{k}_b^{1/4}$, where $\tilde{\epsilon}_O = \epsilon_O/RT$ and $\tilde{k}_b = k_b b_0^2/RT$. The dependence of γ on $\tilde{\epsilon}_O$ (LJ interactions) and $\tilde{k}_b$ (bond flexibility) is consistent with the observation regarding the LJ and bond-stretching virials discussed in previous paragraphs. The role of q_O (charge distribution), however, has not been obvious so far; in fact, as noted earlier, the Coulombic contribution is not one of the major components in the total virial difference (see Figure 5).

TABLE 3: Results of Water Surface Simulation Using a LJ Cutoff Distance, r_c, of 1 nm[a]

water model	γ	ρ_l (g/cm^3)	μ (D)	$\bar{\epsilon}_{\|}$
SPCE-F	64.3	1.019	2.55	125.0
F3C	60.0	0.991	2.46	99.1
expt	71.7[68]	0.9965[69]	2.9[76]	78.4[70]

[a] γ, ρ_l, μ, and $\bar{\epsilon}_{\|}$ are the surface tension, liquid density, dipole moment, and dielectric constant, respectively.

As discussed in the preceding sections, the interfacial water layer may be viewed as a layer in which the water molecules lie almost parallel to the interface and form a lateral structure. The comparison between the SPCE-F model, with $q_O = -0.8476e$, and the SPC-F model, with $q_O = -0.78e$, further indicated that a high surface tension is associated with a tighter, more rigid interfacial water layer. Therefore, in view of the relation depicted in Figure 10, it is possible that the observed alignment and structuring of water molecules at the interface is induced by the charge distribution of the water molecule. In particular, the electrostatic attraction between the oxygen atom in one water molecule and the hydrogen atom in an adjacent water molecule may contribute directly to the stretching of the O−H bond, resulting in a large virial difference due to bond stretching, $\Delta\Xi_b$, and leading to the difference between the SPCE-F and the SPC-F water models shown in Figures 7 and 8a because of the higher charge asymmetry in a SPCE-F water molecule. It must be emphasized that (i) the correlation shown in Figure 10 is not meant to be quantitative, but rather to illustrate the dependence of γ on the various molecular parameters, and (ii) the correlation is applicable only to the ranges of values for q_O, ϵ_O, and k_b shown in Table 1.

LJ Cutoff Distance. As stated earlier, one of the objectives of this study is to compare selected flexible water models using a common set of simulation parameters. Since our focus is on surface tension, a large r_c was used in all simulations to minimize the adverse effect of a small r_c on surface tension reported in the literature. However, as discussed in section 2, the use of a large r_c may introduce inconsistency into some water models. To assess the effect of r_c, not only on surface tension but also on other simulated properties of the water layer, such as density and dielectric constant, two additional simulations were performed with SPCE-F and F3C using the same procedure outlined in section 2 but with $r_c = 1$ nm. As shown in Table 3, the surface tensions in both cases are lowered by approximately 8% compared to those shown in Table 2, thus deviating further from the experimental value of 71.7 mN/m. For SPCE-F, the liquid density (1.019 g/cm^3) is closer to the experimental value, but the dielectric constant also increases further to 125.0. A similar increase in $\bar{\epsilon}_{\|}$ was also observed in F3C. Therefore, although a large r_c (2.45 nm) may introduce some errors in the simulated water density, its use appears justifiable by the improvement observed in both the simulated water surface tension and dielectric constant.

4. Concluding Remarks

Previous molecular dynamics simulations of water surfaces have indicated that the simulated surface tension is affected by both molecular and simulation parameters, such as bond flexibility, simulation time, and the LJ cutoff distance. In the present study, we have performed a systematic comparison of seven flexible water models, using a consistent set of simulation

parameters. These flexible models are based on the harmonic bond-stretching and angle potentials, with variations such as the Urey−Bradley potential used in SPC-Fd and the cubic potential used in the Ferguson model. Our results have shown that contributions from bond stretching and the LJ interactions play a key role in determining the water surface tension. More importantly, these contributions arise from the near-parallel alignment of water molecules with the surface, as well as their lateral structuring in the interfacial liquid layer, which is probably induced by the charge distribution in the water molecule. The insight developed in this study, particularly regarding the roles of various molecular parameters in determining the water surface tension, may have implications on the understanding of surfactant-laden surfaces or interfaces. Indeed, research along this line is already under way.

Acknowledgment. This research was supported by a Discovery Grant from the Natural Sciences and Engineering Research Council of Canada, a New Opportunity Fund from the Canada Foundation for Innovation, and a matching fund from the Nova Scotia Research and Innovation Trust. Computational facilities were provided by the Atlantic Computational Excellence Network (ACEnet) in Canada. D.B. is grateful for the financial support from the DuPont/MIT Alliance.

Supporting Information Available: The molecular dipole moments and hydrogen bond populations are plotted as a function of z', where $z' = [z - 0.5(z_1 + z_2)]/[0.5(z_1 - z_2)]$, and z_1 and z_2 are the locations of the upper and lower GDSs, respectively. Both properties show a small decrease in the interfacial region for all water models considered in this study, which is also observed by Kuo et al. in their simulations using polarizable water models.[77] The decrease in dipole moment (Figure S1) is consistent with the reduced bond stretching in the interfacial region, compared to the bulk (see Figure 8a), while the decrease in hydrogen bond population (Figure S2) is likely related to the transition from liquid density to vapor density across the surface. This material is available free of charge via the Internet at http://pubs.acs.org.

References and Notes

(1) Lu, L.; Berkowitz, M. L. *J. Phys. Chem. B* **2005**, *109*, 21725–21731.
(2) Yang, J.-W.; Lee, Y.-J.; Park, J.-Y.; Kim, S.-J.; Lee, J.-Y. *Eng. Geol.* **2005**, *77*, 243–251.
(3) Li, Z.; Hanlie, H. *Water Res.* **2008**, *42*, 605–614.
(4) Eisenthal, K. B. *Chem. Rev.* **1996**, *96*, 1343–1360.
(5) Goh, M. C.; Hicks, J. M.; Kemnitz, K.; Pinto, G. R.; Bhattacharyya, K.; Eisenthal, K. B. *J. Phys. Chem.* **1988**, *92*, 5074–5075.
(6) Du, Q.; Superfine, R.; Freysz, E.; Shen, Y. R. *Phys. Rev. Lett.* **1993**, *70*, 2313–2316.
(7) Raymond, E. A.; Tarbuck, T. L.; Brown, M. G.; Richmond, G. L. *J. Phys. Chem. B* **2003**, *107*, 546–556.
(8) Ghosh, A.; Smits, M.; Sovago, M.; Bredenbeck, J.; Müller, M.; Bonn, M. *Chem. Phys.* **2008**, *350*, 23–30.
(9) Fan, Y.; Chen, X.; Yang, L.; Cremer, P. S.; Gao, Y. Q. *J. Phys. Chem. B* **2009**, *113*, 11672–11679.
(10) Tian, C. S.; Shen, Y. R. *Chem. Phys. Lett.* **2009**, *470*, 1–6.
(11) Shen, Y. R.; Ostroverkhov, V. *Chem. Rev.* **2006**, *106*, 1140–1154.
(12) Morita, A.; Hynes, J. T. *Chem. Phys.* **2000**, *258*, 371–390.
(13) Morita, A.; Hynes, J. T. *J. Phys. Chem. B* **2002**, *106*, 673–685.
(14) Ji, N.; Ostroverkhov, V.; Tian, C. S.; Shen, Y. R. *Phys. Rev. Lett.* **2008**, *100*, 096102.
(15) Noah-Vanhoucke, J.; Smith, J. D.; Geissler, P. L. *J. Phys. Chem. B* **2009**, *113*, 4065–4074.
(16) Auer, B. M.; Skinner, J. L. *J. Phys. Chem. B* **2009**, *113*, 4125–4130.
(17) Sokhan, V. P.; Tildesley, D. J. *Mol. Phys.* **1997**, *92*, 625–640.
(18) Buch, V. *J. Phys. Chem. B* **2005**, *109*, 17771–17774.
(19) Chacón, E.; Tarazona, P.; Alejandre, J. *J. Chem. Phys.* **2006**, *125*, 014709.
(20) Alejandre, J.; Tildesley, D. J.; Chapela, G. A. *J. Chem. Phys.* **1995**, *102*, 4574–4583.
(21) Yeh, I.-C.; Berkowitz, M. L. *J. Chem. Phys.* **1999**, *111*, 3155–3162.
(22) Abascal, J. L. F.; Vega, C. *J. Chem. Phys.* **2005**, *123*, 234505.
(23) Ismail, A. E.; Grest, G. S.; Stevens, M. J. *J. Chem. Phys.* **2006**, *125*, 014702.
(24) Klauda, J. B.; Wu, X.; Pastor, R. W.; Brooks, B. R. *J. Phys. Chem. B* **2007**, *111*, 4393–4400.
(25) Chen, F.; Smith, P. E. *J. Chem. Phys.* **2007**, *126*, 221101.
(26) Shi, B.; Sinha, S.; Dhir, V. K. *J. Chem. Phys.* **2006**, *124*, 204715.
(27) Lu, Y. J.; Wei, B. *Appl. Phys. Lett.* **2006**, *89*, 164106.
(28) Tironi, I. G.; Brunne, R. M.; van Gunsteren, W. F. *Chem. Phys. Lett.* **1996**, *250*, 19–24.
(29) Teleman, O.; Jönsson, B.; Engström, S. *Mol. Phys.* **1987**, *60*, 193–203.
(30) Wallqvist, A.; Mountain, R. D. Molecular Models of Water: Derivation and Description. In *Reviews in Computational Chemistry*; Lipkowitz, K. B., Boyd, D. B., Eds.; Wiley: New York, 1999; Vol. 13, pp 183−247.
(31) Raabe, G.; Sadus, R. J. *J. Chem. Phys.* **2007**, *126*, 044701.
(32) López-Lemus, J.; Chapela, G. A.; Alejandre, J. *J. Chem. Phys.* **2008**, *128*, 174703.
(33) Mizan, T. I.; Savage, P. E.; Ziff, R. M. *J. Phys. Chem.* **1994**, *98*, 13067–13076.
(34) Toukan, K.; Rahman, A. *Phys. Rev. B* **1985**, *31*, 2643–2648.
(35) Kuchitsu, K.; Morino, Y. *Bull. Chem. Soc. Jpn.* **1965**, *38*, 814–824.
(36) Amira, S.; Spångberg, D.; Hermansson, K. *Chem. Phys.* **2004**, *303*, 327–334.
(37) Carney, G. D.; Curtiss, L. A.; Langhoff, S. R. *J. Mol. Spectrosc.* **1976**, *67*, 371–381.
(38) Wu, Y.; Tepper, H. L.; Voth, G. A. *J. Chem. Phys.* **2006**, *124*, 024503.
(39) Dang, L. X.; Pettitt, B. M. *J. Phys. Chem.* **1987**, *91*, 3349–3354.
(40) Ferguson, D. M. *J. Comput. Chem.* **1995**, *16*, 501–511.
(41) Levitt, M.; Hirshberg, M.; Sharon, R.; Laidig, K. E.; Daggett, V. *J. Phys. Chem. B* **1997**, *101*, 5051–5061.
(42) Zhu, S.-B.; Wong, C. F. *J. Chem. Phys.* **1993**, *98*, 8892–8899.
(43) Vega, C.; de Miguel, E. *J. Chem. Phys.* **2007**, *126*, 154707.
(44) Berendsen, H. J. C.; van der Spoel, D.; van Drunen, R. *Comput. Phys. Commun.* **1995**, *91*, 43–56.
(45) Hess, B.; Kutzner, C.; van der Spoel, D.; Lindahl, E. *J. Chem. Theory Comput.* **2008**, *4*, 435–447.
(46) Mountain, R. D. *J. Phys. Chem. B* **2009**, *113*, 482–486.
(47) Shi, W.-X.; Guo, H.-X. *J. Phys. Chem. B* **2010**, *114*, 6365–6376.
(48) Míguez, J. M.; González-Salgado, D.; Legido, J. L.; Piñeiro, M. M. *J. Chem. Phys.* **2010**, *132*, 184102.
(49) Alejandre, J.; Chapela, G. A. *J. Chem. Phys.* **2010**, *132*, 014701.
(50) Bussi, G.; Donadio, D.; Parrinello, M. *J. Chem. Phys.* **2007**, *126*, 014101.
(51) Lagüe, P.; Pastor, R. W.; Brooks, B. R. *J. Phys. Chem. B* **2004**, *108*, 363–368.
(52) Raschke, T.; Levitt, M. *J. Phys. Chem. B* **2004**, *108*, 13492–13500.
(53) Essmann, U.; Perera, L.; Berkowitz, M.; Darden, T.; Lee, H.; Pedersen, L. G. *J. Chem. Phys.* **1995**, *103*, 8577–8593.
(54) Allen, M. P.; Tildesley, D. J. *Computer Simulation of Liquids*; Oxford University Press: New York, 1987.
(55) Rowlinson, J. S.; Widom, B. *Molecular Theory of Capillarity*; Clarendon Press: Oxford, UK, 1982.
(56) Senapati, S.; Berkowitz, M. L. *Phys. Rev. Lett.* **2001**, *87*, 176101.
(57) Hansen, J. P.; McDonald, I. R. *Theory of Simple Liquids*; Academic Press: London, 1976.
(58) Frenkel, D.; Smit, B. *Understanding Molecular Simulation: From Algorithms to Application*; Academic Press: San Diego, CA, 2002.
(59) Lindahl, E.; Edholm, O. *J. Chem. Phys.* **2000**, *113*, 3882–3893.
(60) Gullingsrud, J.; Schulten, K. *Biophys. J.* **2004**, *86*, 3496–3509.
(61) Patra, M. *Eur. Biophys. J.* **2005**, *35*, 79–88.
(62) Lee, C. Y.; McCammon, J. A.; Rossky, P. J. *J. Chem. Phys.* **1984**, *80*, 4448–4455.
(63) Giovambattista, N.; Debenedetti, P. G.; Rossky, P. J. *J. Phys. Chem. B* **2007**, *111*, 9581–9587.
(64) Giovambattista, N.; Rossky, P. J.; Debenedetti, P. G. *J. Phys. Chem. B* **2009**, *113*, 13723–13734.
(65) Stillinger, F. H.; Rahman, A. *J. Chem. Phys.* **1974**, *60*, 1545–1557.
(66) Sides, S. W.; Grest, G. S.; Lacasse, M.-D. *Phys. Rev. E* **1999**, *60*, 6708–6713.
(67) Ballenegger, V.; Hansen, J.-P. *J. Chem. Phys.* **2005**, *122*, 114711.
(68) Vargaftik, N. B.; Volkov, B. N.; Voljak, L. D. *J. Phys. Chem. Ref. Data* **1983**, *12*, 817–820.
(69) Tanaka, M.; Girard, G.; Davis, R.; Peuto, A.; Bignell, N. *Metrologia* **2001**, *38*, 301–309.

(70) Fernández, D. P.; Mulev, Y.; Goodwin, A. R. H.; Levelt Sengers, J. M. H. *J. Phys. Chem. Ref. Data* **1995**, *24*, 33–69.

(71) Matsumoto, M.; Kataoka, Y. *J. Chem. Phys.* **1988**, *88*, 3233–3245.

(72) Matsuoka, O.; Clementi, E.; Yoshimine, M. *J. Chem. Phys.* **1976**, *64*, 1351–1361.

(73) Carravetta, V.; Clementi, E. *J. Chem. Phys.* **1984**, *81*, 2646–2651.

(74) Recall that the LJ force, $\mathbf{F}_{ij}^{LJ}$, on particle i exerted by particle j can be expressed as $\mathbf{F}_{ij}^{LJ} = 4\epsilon[12(\sigma/r_{ij})^{12}-6(\sigma/r_{ij})^{6}](\mathbf{r}_{ij}/r_{ij}^{2})$, where $\mathbf{r}_{ij} = \mathbf{r}_i - \mathbf{r}_j$. Thus, a positive LJ virial indicates that the repulsive contribution $(12(\sigma/r_{ij})^{12})$ is larger than the attractive contribution $(6(\sigma/r_{ij})^{6})$.

(75) *International Critical Tables of Numerical Data, Physics, Chemistry and Technology*, 1st electronic ed.; Washburn, E. W., Ed.; Knovel: New York, 2003; Vol. III.

(76) Badyal, Y. S.; Saboungi, M.-L.; Price, D. L.; Shastri, S. D.; Haeffner, D. R.; Soper, A. K. *J. Chem. Phys.* **2000**, *112*, 9206–9208.

(77) Kuo, I.-F. W.; Mundy, C. J.; Eggimann, B. L.; McGrath, M. J.; Siepmann, J. I.; Chen, B.; Vieceli, J.; Tobias, D. J. *J. Phys. Chem. B* **2006**, *110*, 3738–3746.

JP1067022